

RESEARCH ARTICLE

Separations: Materials, Devices and Processes

Enhanced one-step purification of C_2H_4 from $C_2H_2/C_2H_4/C_2H_6$ mixtures by fluorinated Zr-MOFJiaqi Liu¹ | Jiafeng Miao¹ | Hao Wang¹  | Yanli Gai² | Jing Li^{1,3}¹Hoffmann Institute of Advanced Materials, Shenzhen Polytechnic, Shenzhen, Guangdong, China²School of Chemistry and Materials Science, Jiangsu Normal University, Xuzhou, Jiangsu, China³Department of Chemistry and Chemical Biology, Rutgers University, Piscataway, New Jersey, USA

Correspondence

Hao Wang and Jing Li, Hoffmann Institute of Advanced Materials, Shenzhen Polytechnic, 7098 Liuxian Blvd., Nanshan, Shenzhen 518055, Guangdong, China.
Email: wanghao@szpt.edu.cn;
jingli@rutgers.edu

Yanli Gai, School of Chemistry and Materials Science, Jiangsu Normal University, Xuzhou, Jiangsu 221116, China.
Email: ylgai@jsnu.edu.cn

Funding information

China Postdoctoral Science Foundation, Grant/Award Number: 2022M713278; National Natural Science Foundation of China, Grant/Award Number: 21901166; Post-Doctoral Foundation Project of Shenzhen Polytechnic, Grant/Award Number: 6022330001K; Science, Technology and Innovation Commission of Shenzhen Municipality, Grant/Award Numbers: JCYJ20190809145615620, RCYX20200714114539243, KCXFZ20211020163818026

Abstract

The extraction of C_2H_4 from $C_2H_6/C_2H_4/C_2H_2$ mixtures is of great significance in the chemical industry for C_2H_4 production but the process remains challenging due to the similarity of these C_2 hydrocarbon species in their molecular size and physical properties. Here, we report the fluorination of a stable Zr-MOF, UiO-66, to fine-tune the pore dimensions and pore functionality. In particular, UiO-66- CF_3 shows notably preferential adsorption of C_2H_6 and C_2H_2 over C_2H_4 , with C_2H_2/C_2H_4 and C_2H_6/C_2H_4 selectivities of 1.4 and 1.9, respectively. Theoretical calculations provide insight into the binding sites of UiO-66- CF_3 for C_2 hydrocarbon adsorption. Breakthrough experiments further confirmed the capability of the material for purification of C_2H_4 from $C_2H_2/C_2H_4/C_2H_6$ ternary mixtures, evidenced by the high purity C_2H_4 (99.9%+) obtained directly from outlet gas.

KEYWORDS

adsorptive separation, ethylene purification, ethylene/ethane/acetylene separation, metal-organic frameworks

1 | INTRODUCTION

Ethylene (C_2H_4), with an annual production capacity of ~200 million metric tons, is the most important feedstock in petrochemical industry.^{1–3} Currently, ethylene is usually produced by thermal cracking of naphtha or ethane, where ethane (C_2H_6) and acetylene (C_2H_2) will unavoidably co-exist as by-products.^{4,5} Therefore, the removal of C_2H_6 and C_2H_2 from the cracked steam to yield polymer-grade ethylene (>99.9% purity) is a crucial process. However, discrimination of the three components is very challenging due to the similarity of their physico-chemical properties (Table S1).^{6,7} At present, C_2H_2 in the cracked gas needs to be removed first, by catalytic hydrogenation or solvent

extraction, and then C_2H_6 and C_2H_4 are separated by cryogenic distillation under high pressure with more than a hundred trays.^{8,9} The entire purification process is complicated and energy insensitive and thus, it is necessary and urgent to develop a simpler separation approach with lower energy input for C_2H_4 purification.¹⁰ Among various technologies, adsorptive separation based on porous adsorbents has been considered a promising method because it can be operated under mild conditions with suppressed energy consumption.^{11,12} However, one-step purification of C_2H_4 from $C_2H_2/C_2H_4/C_2H_6$ mixture through adsorptive separation has stringent requirements on the pore structure and binding sites of the adsorbents to ensure they preferentially adsorb C_2H_6 and C_2H_2 over C_2H_4 . The main reason is that the quadrupole moment and kinetic

Jiaqi Liu and Jiafeng Miao have contributed equally to this study.

diameter of C_2H_4 (1.5×10^{-26} esu cm^2 and 4.1 Å) lie between those of C_2H_2 (7.2×10^{-26} esu cm^2 and 3.3 Å) and C_2H_6 (0.65×10^{-26} esu cm^2 and 4.4 Å). This prevents most adsorbents from one-step purification of C_2H_4 from C_2 ternary mixtures through molecular sieving or thermodynamically driven mechanism. In this context, metal-organic frameworks (MOFs) with attractive characteristics, including diverse topologies and adjustable pore size and functionality, show great prospects in addressing this challenging separation.^{13,14} While a number of MOFs have been developed and used to separate C_2H_4 from binary C_2H_2/C_2H_4 or C_2H_6/C_2H_4 mixtures, few of them are capable of direct extraction of C_2H_4 from C_2 ternary mixtures.^{15–18} To this end, we believe it is possible to obtain optimal adsorbents that are suitable for one-step purification of C_2H_4 from ternary $C_2H_2/C_2H_4/C_2H_6$ mixtures by fine engineering pore dimensions and functionality of MOFs through the incorporation of proper functional groups.

In an effort to evaluate the effect of pore surface fluorination on the separation of light hydrocarbon, Wu et al.¹⁹ recently synthesized three Cu(II)-MOFs constructed from isonicotinic acid and its fluorinated analogue, 3-fluoro-isonicotinic acid. Their study shows that the polar F sites within the confined pores serve as strong binding sites for alkyne through C-H-F hydrogen bonds, resulting in notably improved C_2H_2/C_2H_4 and C_3H_4/C_3H_6 selectivity. More recently, Guo et al.²⁰ prepared a fluorinated QMOF-2 (denoted as QMOF-2F) and investigated the influence of the fluorine-functionalization on light hydrocarbons separation. The results indicate that the F sites play a significant role in boosting the preferential interactions with C_2 -hydrocarbons than CH_4 . Lately, Zhang et al.²¹ realized the one-step purification of C_2H_4 from ternary $C_2H_2/C_2H_4/C_2H_6$ mixtures by constructing anion-pillared hybrid ultramicroporous materials, $CuTiF_6$ -TPPY, where the low-polarity surface provided by the porphyrin rings can selectively adsorb C_2H_6 and the abundant TiF_6^{2-} anions can effectively capture C_2H_2 . The studies reported thus far provide strong evidence that fluorine groups can influence the pore surface functionality of the adsorbents, which may enhance their capability for selective adsorption of C_2H_6 and C_2H_2 over C_2H_4 .²² Therefore, rationally designed and precisely engineered stable fluorinated MOFs could be

excellent adsorbents to achieve one-step purification of C_2H_4 from ternary $C_2H_2/C_2H_4/C_2H_6$ mixtures.

The prototype Zr-based MOF, UiO-66, is built on a 12-connected hexanuclear SBU $Zr_6O_4(OH)_4(COO)_{12}$ and 2-connected dicarboxylate linker terephthalate. It possesses two types of cage-like pores with tetrahedral and octahedral geometry that are interconnected through an equilateral triangular window (Figure S1).^{23,24} Thus the pore aperture and binding sites of the MOF can be finely modified by incorporating organic ligands with different functional groups.

In this study, we prepared two fluorinated MOFs UiO-66- CF_3 and UiO-66- $(CF_3)_2$ by incorporating one or two $-CF_3$ groups onto the organic linker of UiO-66 (Figure 1). The influence of fluorine-functionalization on $C_2H_2/C_2H_4/C_2H_6$ separation was thoroughly investigated experimentally and through theoretical calculations. Single-component adsorption revealed that UiO-66- CF_3 exhibits notably higher C_2H_2 and C_2H_6 adsorption capacities than that of C_2H_4 , reaching adsorption selectivities of 1.4 and 1.9 for C_2H_2/C_2H_4 and C_2H_6/C_2H_4 , respectively. Multicomponent column breakthrough experiments confirm the capability of UiO-66- CF_3 for one-step purification of C_2H_4 from $C_2H_2/C_2H_4/C_2H_6$ ternary mixtures. Furthermore, grand canonical Monte Carlo (GCMC) calculations were performed to investigate the optimal adsorption sites and to explain the underlying separation mechanism.

2 | MATERIALS AND METHODS

2.1 | Synthesis of MOFs

Synthesis of UiO-66: zirconium(IV) chloride (116.5 mg, 0.5 mmol) and 1,4-dicarboxybenzene (49.8 mg, 0.3 mmol) were dissolved in DMF (5 ml) in a 20 ml Teflon-lined autoclave. The mixture was sonicated for 30 min before being placed in a 120 °C oven for 2 days. The white powder was obtained by filtration. The crystals were washed by DMF (3×10 ml) and exchanged with methanol through a Soxhlet extractor

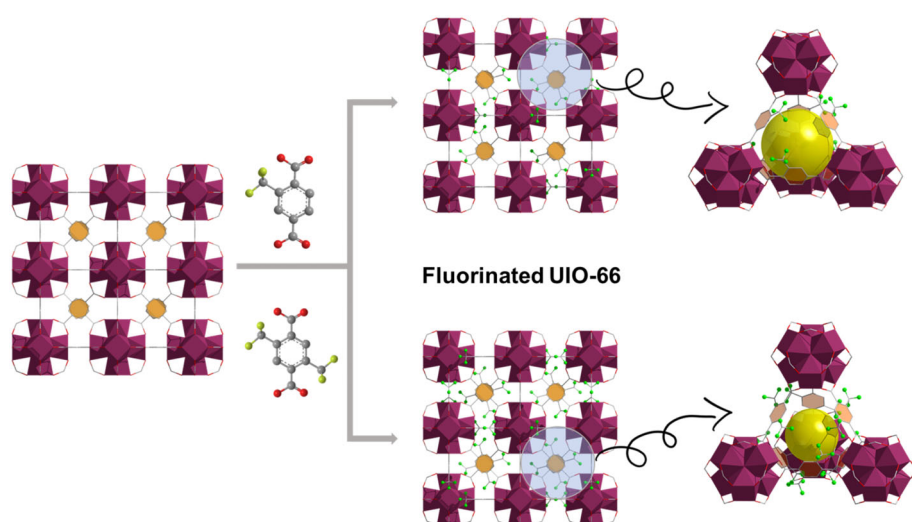


FIGURE 1 Crystal structures of the fluorine-functionalized UiO-66.

for 1 day. The solvent-exchanged sample was dried at 120 °C under vacuum to yield activated sample.

Synthesis of UiO-66-CF₃: zirconium(IV) chloride (116.5 mg, 0.5 mmol) and 2-(trifluoromethyl)terephthalic acid (70.20 g, 0.3 mmol) was dissolved in DMF (5 ml) in a 20 ml Teflon-lined autoclave and formic acid (0.3 ml) was added to the solution. The mixture was sonicated for 30 min before being placed in a 150 °C oven for 2 days. The white powder was obtained by filtration. The crystals were washed by DMF (3 × 10 ml) and exchanged with methanol through a Soxhlet extractor for 1 day. The solvent-exchanged sample was dried at 120 °C under vacuum to yield activated sample.

Synthesis of UiO-66-(CF₃)₂: zirconium(IV) chloride (116.5 mg, 0.5 mmol) and 2,5-bis(trifluoromethyl)terephthalic acid (90.6 mg, 0.3 mmol) were dissolved in DMF (5 ml) in a 20 ml Teflon-lined autoclave and formic acid (0.9 ml) was added to the solution. The mixture was sonicated for 30 min before being placed in a 150 °C oven for 2 days. The white powder was obtained by filtration. The crystals were washed by DMF (3 × 10 ml) and exchanged with methanol through a Soxhlet extractor for 1 day. The solvent-exchanged sample was dried at 120 °C under vacuum to yield activated sample.

2.2 | General characterizations

Powder X-ray diffraction patterns were recorded on a Bruker D8 Advance with Cu K α radiation ($\lambda = 1.5406$ Å). Data were collected at room temperature at $2\theta = 5$ –40°. Thermogravimetric analysis was carried out on a TGA 550 (TA Instruments) analyzer. For each run, 3–5 mg of sample was heated from room temperature to 600 °C at a ramp rate of 10 °C/min. C₂H₂, C₂H₄, and C₂H₆ adsorption at 298 K and 278 K were measured on a Quantachrome Autosorb-iQ analyzer. N₂ adsorption isotherms at 77 K were measured on a Micromeritics 3Flex analyzer. For each adsorption experiment, ~100 mg of MOF sample was activated overnight before data collection.

2.3 | Isostatic heat of adsorption

To determine the affinity between the scaffold and the adsorbates, the Clausius–Clapeyron equation was employed to calculate the adsorption heat for gas, which was defined as follows:

$$Q_{st} = -RT^2 \left(\frac{\partial \ln P}{\partial \ln T} \right)_q \quad (1)$$

where Q_{st} represents the adsorption heat of gas, P , T , and q represent the pressure, temperature, and adsorption amount, under adsorption measurement conditions, and R is the universal gas constant.

2.4 | Adsorption selectivity calculation

The dual site Langmuir–Freundlich isotherm model was adopted to fit the adsorption isotherms of C₂H₂/C₂H₄/C₂H₆, which was described as follows:

$$q = q_{A,sat} \frac{b_A P^{v_A}}{1 + b_A P^{v_A}} + q_{B,sat} \frac{b_B P^{v_B}}{1 + b_B P^{v_B}} \quad (2)$$

with T-dependent parameters b_A , and b_B

$$b_A = b_{AO} \exp\left(\frac{E_A}{RT}\right); b_B = b_{BO} \exp\left(\frac{E_B}{RT}\right) \quad (3)$$

where q represents the adsorption amount of adsorbents with units of mol·kg^{−1}, $q_{A,sat}$ and $q_{B,sat}$ represents the saturated adsorption amount for adsorption sites A and B, respectively, b_A and b_B are constants for species i at adsorption sites A and B, respectively, p is the total pressure of the bulk gas at the adsorption equilibrium, and v_A and v_B are the Freundlich exponent for sites A and B, respectively.

Taking C₂H₆/C₂H₄ mixtures as an example, the IAST selectivity is defined by²⁵:

$$S_{ads} = \frac{q_1/q_2}{y_1/y_2} \quad (4)$$

where q_1 and q_2 represent the adsorption amounts of C₂H₆ and C₂H₄ upon the sample under equilibrium conditions, which is usually expressed with units of mmol·g^{−1}, y_1 and y_2 are the corresponding mole fractions in the gas phase for the mixtures.

2.5 | GCMC simulation details

The GCMC simulations were carried out with the Sorption program (BIOVIA Material studio 8.0) to investigate the interactions between the framework and C₂ gas molecules. In our work, the crystal structure of UiO-66-CF₃ was chosen for related simulations without further geometry optimization. A cutoff radius of 12.5 Å was used to handle the nonbonding interactions, and the Ewald & Group summation method was applied to calculate the long-range electrostatic interactions. Each state point of GCMC simulations contained 1×10^7 steps to guarantee equilibration followed by 1×10^7 steps to sample the required thermodynamics properties. The framework was treated as rigid structure by fixing atoms at their crystallographic positions, which has been proven to yield accurate results in a large variety of GCMC studies. UFF force field was adopted to describe the LJ parameters for the atoms in simulations. Partial charges for all atoms were derived from QEq method and QEq_neutral 1.0 parameter.

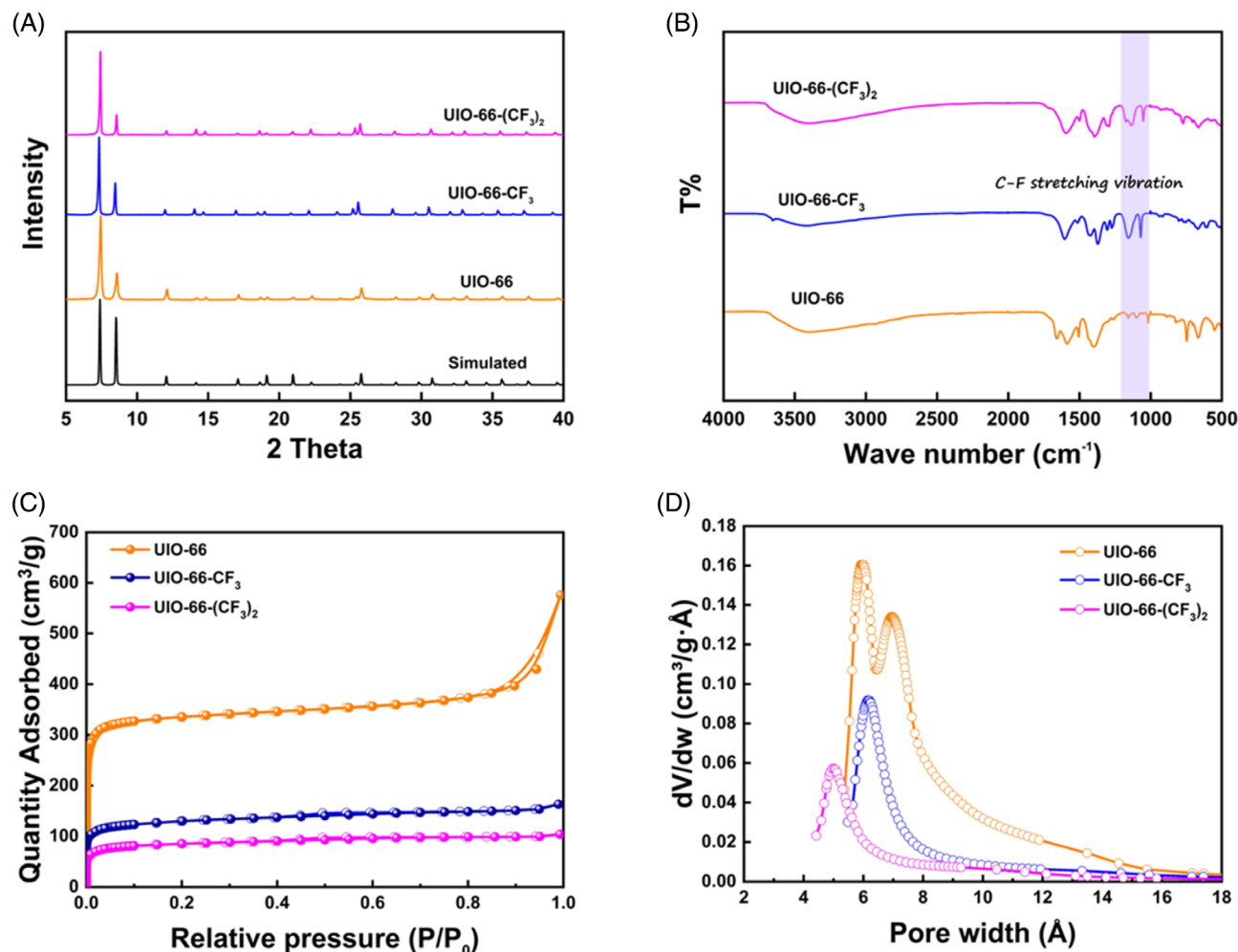


FIGURE 2 (A) PXRD patterns (B) FTIR spectra (C) N₂ adsorption-desorption isotherms at 77 K, (D) pore size distribution by Horvath-Kawazoe method for UiO-66, UiO-66-CF₃, and UiO-66-(CF₃)₂.

2.6 | Breakthrough measurements

Breakthrough tests were carried out in an auto mixed-gas breakthrough apparatus (3P Mixsorb S). The mass of UiO-66, UiO-66-CF₃ and UiO-66-(CF₃)₂ filled into the column (I.D. 6 mm, length 100 mm) was 0.40, 0.86, and 0.75 g, respectively. The adsorbents were activated at 120 °C for 5 h under helium purging (10 ml/min). When the temperature cooled down to 25 °C, helium flow was stopped and the feed mixed gases (C₂H₆/C₂H₄, 10/90 or C₂H₂/C₂H₄/C₂H₆, 1/90/9; v/v) at a flow rate of 1 ml/min were introduced to the adsorption column. The outlet gas was analyzed by using a mass spectrometer (MKS circus 3). After the adsorption reached dynamic equilibrium, the column was purged with helium (10 ml/min) at 120 °C for 1 h for regeneration.

The C₂H₄ purity and productivity was calculated by the following method: the gas breakthrough gas amount (q_i) was calculated by integrating the breakthrough curve $f(t)$ as the following equation.

$$q_i = \frac{\int_0^{t_0} f(t) dt}{m} \times c_i \quad (5)$$

where m represents the adsorbent mass and c_i represents the fraction of components in the feed gas mixture.

And then the purity (c) of breakthrough gas was calculated by the following equation.

$$c = \frac{q_{C_2H_4}}{q_{C_2H_2} + q_{C_2H_6} + q_{C_2H_4}} \quad (6)$$

3 | RESULTS AND DISCUSSION

3.1 | Material synthesis and characterization

UiO-66, UiO-66-CF₃, and UiO-66-(CF₃)₂ were synthesized according to the previously reported procedures with slight modification,^{26,27} and the phase purity was confirmed by comparing the synthesized and simulated powder X-ray diffraction (PXRD) patterns which show a nearly perfect match (Figure 2A). The existence of -CF₃ groups was supported by Fourier transform infrared (FTIR) spectroscopic analysis. As shown in Figure 2B, a strong band attributed to C-F stretch

vibrations is present in the IR spectra of UiO-66- CF_3 (1157.75 and 1071.25 cm^{-1}) and UiO-66- $(\text{CF}_3)_2$ (1133.75 and 1053.25 cm^{-1}) but is absent in that of UiO-66. Thermogravimetric (TG) analysis revealed that all the solvent-exchanged samples can be fully desolvated at 393 K and possess high thermal stability (UiO-66: ca. 723 K UiO-66- CF_3 : ca. 643 K UiO-66- $(\text{CF}_3)_2$: ca. 623 K, Figure S2). N_2 adsorption-desorption isotherms at 77 K were employed to investigate the specific surface area and porosity of the materials. As shown in Figure 2C, all three compounds exhibit typically reversible type-I adsorption profiles, indicating their microporous nature. The specific surface areas of UiO-66, UiO-66- CF_3 , and UiO-66- $(\text{CF}_3)_2$ were calculated to be 1299.19, 487.46, and $279.94\text{ m}^2/\text{g}$, respectively, by Brunauer-Emmett-Teller (BET) method, showing a gradually decreasing trend, which is caused by the incorporation of $-\text{CF}_3$ groups. Moreover, the pore size distribution was also altered by the CF_3 groups. As shown in Figure 2D, UiO-66 has a pore size centered at 0.64 nm, whereas for UiO-66- CF_3 and UiO-66- $(\text{CF}_3)_2$ the values are reduced to 0.61 and 0.50 nm, respectively. Apparently, through the fluorination of UiO-66, its pore dimensions and pore environment have been precisely tuned, which encourages us to explore its $\text{C}_2\text{H}_2/\text{C}_2\text{H}_4/\text{C}_2\text{H}_6$ separation performance.

3.2 | Gas adsorption and separation performance

The single-component adsorption-desorption isotherms were collected at 273 and 298 K for C_2H_2 , C_2H_4 , and C_2H_6 up to 1 bar on

three materials (Figures 3A–C and S3). UiO-66 with the largest pore size and BET surface area exhibits the highest adsorption capacity for C_2H_2 , C_2H_4 , and C_2H_6 of 64.77, 53.63, and $54.37\text{ cm}^3/\text{g}$, respectively. UiO-66- CF_3 with intermediate pore size possesses a relatively lower adsorption capacity of C_2 molecules to UiO-66. Nevertheless, its adsorption amounts of C_2H_2 , C_2H_4 , and C_2H_6 are 33.70, 25.36, and $30.91\text{ m}^3/\text{g}$, respectively, showing notably preferential adsorption of C_2H_2 and C_2H_6 over C_2H_4 . This should be attributed to the incorporated $-\text{CF}_3$ that results in a more nonpolar surface wherein the binding strength of C_2H_2 and C_2H_6 is enhanced compared with that of C_2H_4 . This hypothesis can be well confirmed by the experimental isosteric heat of adsorption (Q_{st}) calculated by the Clausius-Clapeyron relation using isotherms at 273 and 298 K (Figure S4). As shown in Figure 3D, the initial Q_{st} values of UiO-66- CF_3 for C_2H_2 (24.27 kJ/mol) and C_2H_6 (24.32 kJ/mol) is notably higher than that of C_2H_4 (22.18 kJ/mol). In contrast, UiO-66- $(\text{CF}_3)_2$ with the narrowest pore size exhibits similar and lowest adsorption amounts/ Q_{st} for C_2 hydrocarbons making it difficult to discriminate the three C_2 molecules. This could be due to the excessively contracted pore size and more $-\text{CF}_3$ can weaken the binding strength of all three C_2 molecules significantly, as evidenced by the very low Q_{st} values.

The ideal adsorbed solution theory (IAST) was used to evaluate the separation performance of $\text{C}_2\text{H}_2/\text{C}_2\text{H}_4$ and $\text{C}_2\text{H}_6/\text{C}_2\text{H}_4$ for equimolar gas mixtures at 298 K and 1 bar. The results are shown in Figure 3E, after fitting the single component adsorption isotherms at 298 K to the dual sites Langmuir-Freundlich equation (fitting

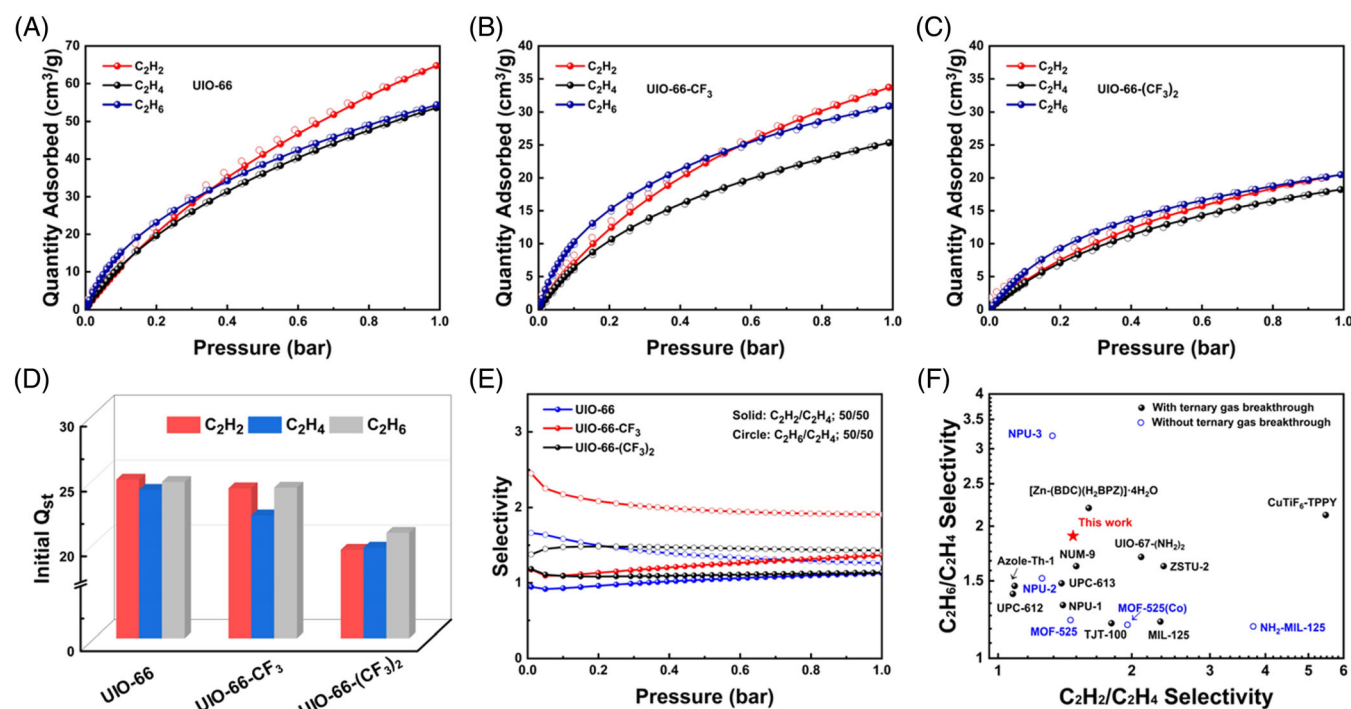


FIGURE 3 The $\text{C}_2\text{H}_2/\text{C}_2\text{H}_4/\text{C}_2\text{H}_6$ adsorption isotherms at 298 K on (A) UiO-66, (B) UiO-66- CF_3 , and (C) UiO-66- $(\text{CF}_3)_2$; (D) Initial isosteric heat of adsorption (Q_{st}) of C_2H_2 , C_2H_4 , and C_2H_6 on three materials; (E) IAST predicted equimolar $\text{C}_2\text{H}_2/\text{C}_2\text{H}_4$ and $\text{C}_2\text{H}_6/\text{C}_2\text{H}_4$ mixtures at 298 K; and (F) Comparison of C_2 separation performance of reported adsorbents based on IAST selectivity.

parameters listed in Table S2). The adsorption selectivity values for C_2H_2/C_2H_4 and C_2H_6/C_2H_4 on UiO-66- CF_3 were calculated to be 1.4 and 1.9, significantly higher than that of UiO-66 (1.1 and 1.3) and UiO-66- $(CF_3)_2$ (1.1 and 1.4). The values are also comparable to the benchmark adsorbent capable of one-step purification of C_2H_4 from the $C_2H_2/C_2H_4/C_2H_6$ mixture (Figure 3F).^{7,8,21,28–35} The

selectivities of C_2H_2/C_2H_4 (1/99; v/v) and C_2H_6/C_2H_4 (10/90; v/v) were also calculated which are close to the values for equimolar mixtures (Figure S5). Therefore, our results indicate that properly optimizing the pore size and pore functionality of MOFs can efficiently enhance the favored adsorption of C_2H_2 and C_2H_6 over C_2H_4 .

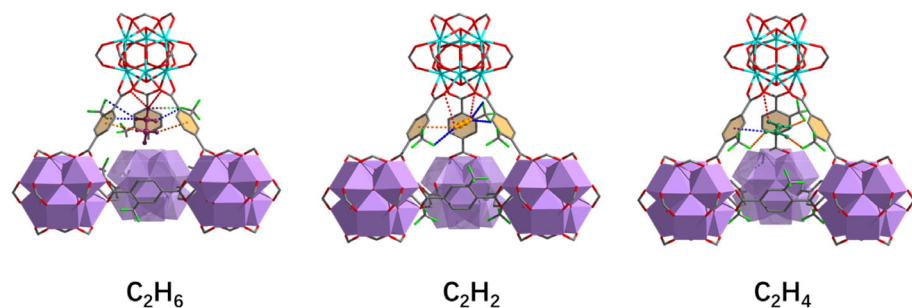


FIGURE 4 The adsorption sites and interactions between C_2H_6 , C_2H_2 , and C_2H_4 with the framework of UiO-66- CF_3 .

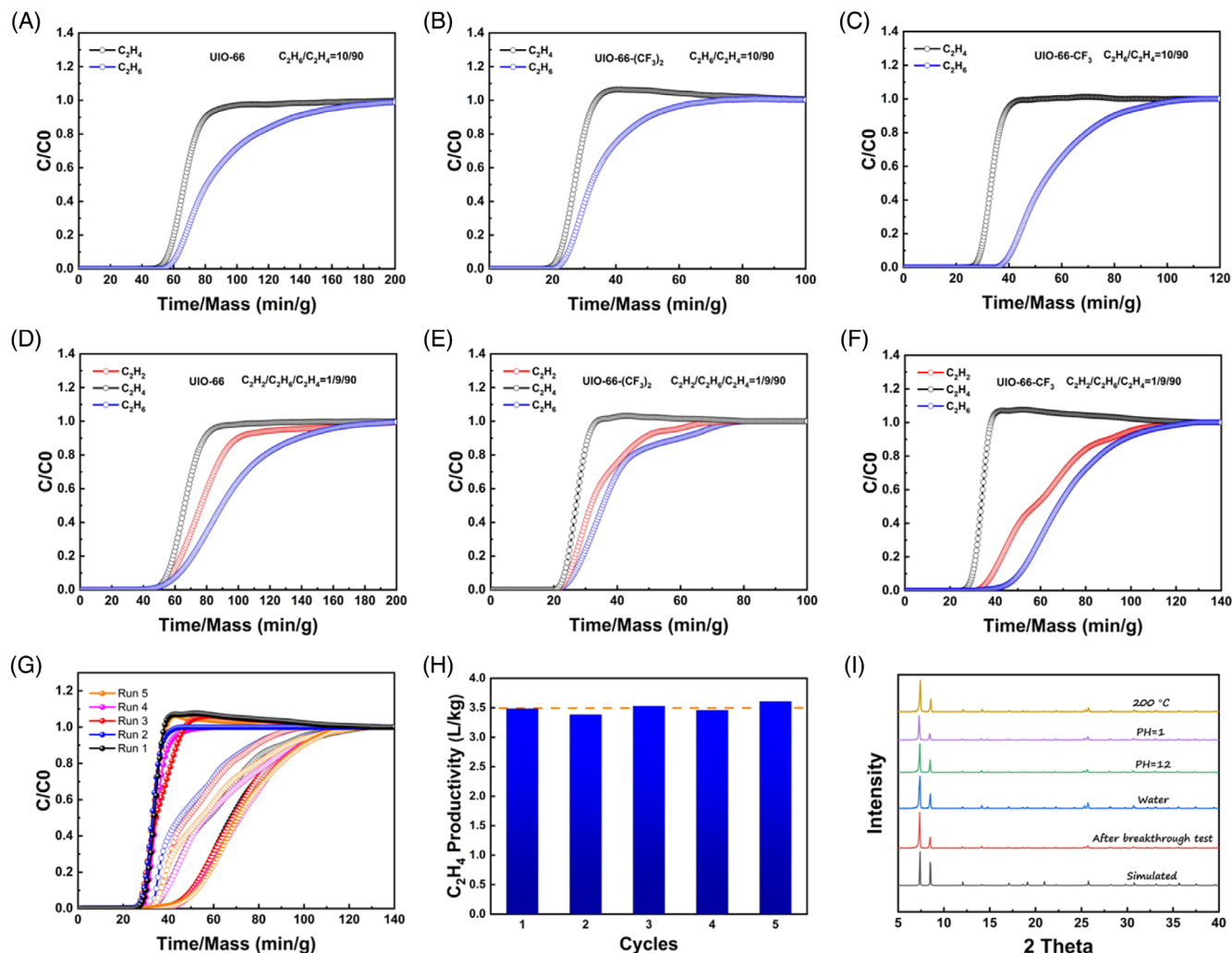


FIGURE 5 Dynamic breakthrough for binary C_2H_6/C_2H_4 mixture (10/90, v/v) at 298 K on (A) UiO-66, (B) UiO-66- $(CF_3)_2$, and (C) UiO-66- CF_3 , breakthrough curves for ternary $C_2H_2/C_2H_4/C_2H_6$ mixture (1/90/9, v/v/v) at 298 K on (D) UiO-66, (E) UiO-66- $(CF_3)_2$ and (F) UiO-66- CF_3 , (G) five consecutive breakthrough cycles of UiO-66- CF_3 for ternary $C_2H_2/C_2H_4/C_2H_6$ mixture (1/90/9, v/v/v) at 298 K, (H) the productivity of C_2H_4 of five consecutive cycles, and (I) PXRD patterns of UiO-66- CF_3 treated in different environments.

3.3 | Computational simulation studies

The grand canonical Monte Carlo (GCMC) simulations on UiO-66- CF_3 were performed to investigate the interactions between the host frameworks and C_2 molecules. The density distribution maps at 101 kPa and 298 K revealed that the primary C_2 adsorption sites are located in the tetrahedral cage pockets (Figure S6). To clearly show the adsorption site and interactions, only one adsorbed C_2 gas molecule on the primary adsorption site is shown in Figure 4 and the interactions are listed in Table S3 in detail. The C_2H_6 molecule makes the closest contacts to the MOF, including two $\text{C-H}\cdots\pi$ (2.93–2.94 Å) interactions with two phenyl rings, three $\text{C-H}\cdots\text{F}$ ($\text{H}\cdots\text{F}$, 2.61–3.26 Å) interactions with $-\text{CF}_3$ groups and two $\text{C-H}\cdots\text{O}$ ($\text{H}\cdots\text{O}$, 2.61–2.76 Å) interactions with one carboxylate group. The C_2H_2 molecule is involved in one $\text{C-H}\cdots\pi$ ($\text{H}\cdots\pi$, 3.2 Å), three $\text{C-H}\cdots\text{F}$ ($\text{H}\cdots\text{F}$, 2.50, 2.85 and 3.13 Å) and two $\text{C-H}\cdots\text{O}$ ($\text{H}\cdots\text{O}$, 2.66, 3.03 Å) interactions. As for C_2H_4 , it has the fewest close contacts with the framework and the $\text{C-H}\cdots\text{F}$ ($\text{H}\cdots\text{F}$, 3.26, 2.64 and 2.61 Å) distances are longer than those of C_2H_2 . Thus, the simulated binding interactions are consistent with the experimental Q_{st} values in the order of $\text{C}_2\text{H}_6 > \text{C}_2\text{H}_2 > \text{C}_2\text{H}_4$.

3.4 | Dynamic breakthrough experiments

To evaluate the separation performance of the compounds for actual gas mixtures, dynamic column breakthrough experiments were performed for UiO-66, UiO-66- CF_3 , and UiO-66- $(\text{CF}_3)_2$. In a typical breakthrough experiment at 298 K, a mixture of $\text{C}_2\text{H}_2/\text{C}_2\text{H}_4/\text{C}_2\text{H}_6$ (1/90/9; v/v) or $\text{C}_2\text{H}_6/\text{C}_2\text{H}_4$ (10/90; v/v) at a total gas pressure of 1 bar was passed through the packed adsorbent column, and the outlet gas signal was detected by a mass spectrometer. As shown in Figure 5A, B, D, E, UiO-66 and UiO-66- $(\text{CF}_3)_2$ can barely extract C_2H_4 from binary or ternary mixture indicated by the very close breakthrough time of the gases. As for UiO-66- CF_3 , with $\text{C}_2\text{H}_6/\text{C}_2\text{H}_4$ (10/90; v/v) binary mixture as a feed, C_2H_4 breakthrough occurred first at ca. 26th min/g, followed by C_2H_6 at ca. 35th min/g, establishing its ability to produce polymer-grade ethylene of 4.24 L/kg (Figure 5C). Furthermore, dynamic breakthrough experiments with $\text{C}_2\text{H}_2/\text{C}_2\text{H}_4/\text{C}_2\text{H}_6$ (1/90/9; v/v) ternary mixture were performed, and three gases broke out successively in the sequence of C_2H_4 (ca. 25th min/g)- C_2H_2 (ca. 31st min/g)- C_2H_6 (ca. 34th min/g) (Figure 5F). During the breakthrough interval between C_2H_4 and C_2H_2 , polymer-grade C_2H_4 was harvested with a dynamic capacity of 3.49 L/kg, indicating its good performance for one-step C_2H_4 purification from the ternary gas mixture. The breakthrough experiment under 50% RH humidity was also carried out to test the water resistance of UiO-66- CF_3 . As shown in Figure S7, the breakthrough time under humid environment is slightly shorter than that in a dry environment. The C_2H_4 productivity decreased slightly from 3.49 to 3.32 L/kg, indicating the separation performance was mainly retained under humid conditions. For practical applications, recyclability of the adsorbent is important, thus the adsorption bed was regenerated

under helium (He) flow (10 ml/min) under 393 K, and five consecutive breakthrough cycles were carried out. The results show that breakthrough curves, C_2H_4 productivity, and PXRD patterns taken after the experiments remained nearly the same (Figure 5G–I). The N_2 adsorption isotherm at 77 K of the samples after the breakthrough was tested and shown in Figure S8. The results further proved the structural integrity of UiO-66- CF_3 with evidence of nearly non-changed adsorption capacity and BET surface area (490.49 m^2/g). Moreover, the thermal and chemical stability of UiO-66- CF_3 was also evaluated by exposing the material to various treatments including 200 °C atmosphere, water, HCl (pH = 1) and NaOH (pH = 12) aqueous solutions for 3 days. From the PXRD patterns plotted in Figure 5I, it is clear that UiO-66- CF_3 maintained its structural integrity under all these conditions, proving that it can meet the demand for industrial adsorption separations.

4 | SUMMARY

The quest for optimal adsorbents for one-step separation of C_2H_4 from $\text{C}_2\text{H}_2/\text{C}_2\text{H}_4/\text{C}_2\text{H}_6$ mixtures represents an important but challenging task in the chemical industry. In this work, to fine-tune the pore structure and environment of the prototype MOF UiO-66, we prepared two fluorinated analogues, denoted as UiO-66- CF_3 and UiO-66- $(\text{CF}_3)_2$. The influence of pore size and the electronic environment on $\text{C}_2\text{H}_2/\text{C}_2\text{H}_4/\text{C}_2\text{H}_6$ separation was investigated comprehensively by both experimental and theoretical methods. In particular, we found that UiO-66- CF_3 holds excellent $\text{C}_2\text{H}_2/\text{C}_2\text{H}_4$ and $\text{C}_2\text{H}_6/\text{C}_2\text{H}_4$ selectivity. Dynamic breakthrough experiments with ternary and binary C_2 gas mixtures confirmed the capability of direct production of high-purity C_2H_4 (99.9%) by UiO-66- CF_3 . Moreover, sorbent-sorbate interactions were analyzed by GCMC simulations. By studying the influence of fluorine groups on the adsorption and separation of C_2 molecules, we have gained useful information on the structure-adsorption relationship, which may further guide the design of high-performance adsorbents for the purification of C_2H_4 .

AUTHOR CONTRIBUTIONS

Jiaqi Liu: Investigation (lead); project administration (lead); writing – original draft (lead). **Jiafeng Miao:** Investigation (equal); methodology (equal). **Hao Wang:** Conceptualization (lead); supervision (lead); writing – review and editing (lead). **Yanli Gai:** Methodology (equal); supervision (equal); validation (equal). **Jing Li:** Conceptualization (lead); supervision (lead); writing – review and editing (lead).

ACKNOWLEDGMENTS

This work is financially supported by the National Natural Science Foundation of China (21901166) and Shenzhen Science and Technology Program (No. JCYJ20190809145615620, RCYX20200714114539243, KCXFZ20211020163818026), Post-doctoral Foundation Project of Shenzhen Polytechnic (6022330001K) and China Postdoctoral Science Foundation (2022M713278).

CONFLICT OF INTEREST

The authors declare no conflict of interest.

DATA AVAILABILITY STATEMENT

The data that supports the findings of this study are available in the supplementary material of this article

ORCID

Hao Wang  <https://orcid.org/0000-0001-7732-778X>

REFERENCE

1. Zeng H, Xie XJ, Xie M, et al. Cage-interconnected metal-organic framework with tailored apertures for efficient C_2H_6/C_2H_4 separation under humid conditions. *J Am Chem Soc.* 2019;141(51):20390-20396.
2. Lysova AA, Samsonenko DG, Kovalenko KA, Nizovtsev AS, Dybtsev DN, Fedin VP. A series of mesoporous metal-organic frameworks with tunable window sizes and exceptionally high ethane over ethylene adsorption selectivity. *Angew Chem Int Ed Engl.* 2020;59(46):20561-20567.
3. Chu S, Cui Y, Liu N. The path towards sustainable energy. *Nat Mater.* 2017;16(1):16-22.
4. Sadrameli SM. Thermal/catalytic cracking of hydrocarbons for the production of olefins: a state-of-the-art review I: thermal cracking review. *Fuel.* 2015;140:102-115.
5. Zhang Y, Wu J-h, Zhang D-k. Cracking of simulated oil refinery off-gas over a coal char, petroleum coke, and quartz. *Energy Fuel.* 2008;22(2):1142-1147.
6. Li JR, Kuppler RJ, Zhou HC. Selective gas adsorption and separation in metal-organic frameworks. *Chem Soc Rev.* 2009;38:1477.
7. Liu P, Wang Y, Chen Y, et al. Construction of saturated coordination titanium-based metal-organic framework for one-step $C_2H_2/C_2H_6/C_2H_4$ separation. *Sep Purif Technol.* 2021;276:119284.
8. Gu XW, Wang JX, Wu E, et al. Immobilization of Lewis basic sites into a stable ethane-selective MOF enabling one-step separation of ethylene from a ternary mixture. *J Am Chem Soc.* 2022;144(6):2614-2623.
9. Belohlav Z, Zamostny P, Herink T. The kinetic model of thermal cracking for olefins production. *Chem Eng Process.* 2003;42(6):461-473.
10. Sholl DS, Lively RP. Seven chemical separations to change the world. *Nature.* 2016;532(7600):435-437.
11. He Y, Krishna R, Chen B. Metal-organic frameworks with potential for energy-efficient adsorptive separation of light hydrocarbons. *Energ Environ Sci.* 2012;5(10):9107-9120.
12. Zhou D-D, Zhang J-P. On the role of flexibility for adsorptive separation. *Acc Chem Res.* 2022;55(20):6010-6017.
13. Lin R-B, Xiang S, Xing H, Zhou W, Chen B. Exploration of porous metal-organic frameworks for gas separation and purification. *Coord Chem Rev.* 2019;378:87-103.
14. Lin R-B, Xiang S, Zhou W, Chen B. Microporous metal-organic framework materials for gas separation. *Chem.* 2020;6(2):337-363.
15. Xiang SC, Zhang Z, Zhao CG, et al. Rationally tuned micropores within enantiopure metal-organic frameworks for highly selective separation of acetylene and ethylene. *Nat Commun.* 2011;2:204.
16. Chen H, Zhuang GL, Fan L, Zhang X, Gao LN, Sun D. A highly robust heterometallic Tb(III)/Ni(II)-organic framework for C_2 hydrocarbon separation and capture. *Chem Commun (Camb).* 2020;56(13):2047-2050.
17. Liao PQ, Zhang WX, Zhang JP, Chen XM. Efficient purification of ethylene by an ethane-trapping metal-organic framework. *Nat Commun.* 2015;6:8697.
18. Yang H, Wang Y, Krishna R, et al. Pore-space-partition-enabled exceptional ethane uptake and ethane-selective ethane-ethylene separation. *J Am Chem Soc.* 2020;142(5):2222-2227.
19. Wu X-Q, Liu J-H, He T, Zhang P-D, Yu J, Li J-R. Understanding how pore surface fluorination influences light hydrocarbon separation in metal-organic frameworks. *Chem Eng J.* 2021;407:127183.
20. Guo Y, Liang C, Zhang CC, et al. Enhanced sieving of C_2 -hydrocarbon from methane by Fluoro-functionalization of In-MOF with robust stability. *Chem Asian J.* 2022;17(1):e202101220.
21. Zhang P, Zhong Y, Zhang Y, et al. Synergistic binding sites in a hybrid ultramicroporous material for one-step ethylene purification from ternary C_2 hydrocarbon mixtures. *Sci Adv.* 2022;8(23):eabn9231.
22. Ebadi Amooghin A, Sanaeepour H, Luque R, Garcia H, Chen B. Fluorinated metal-organic frameworks for gas separation. *Chem Soc Rev.* 2022;51(17):7427-7508.
23. Cavka JH, Jakobsen S, Olsbye U, et al. A new zirconium inorganic building brick forming metal organic frameworks with exceptional stability. *J Am Chem Soc.* 2008;130(42):13850-13851.
24. Winarta J, Shan B, McIntyre SM, et al. A decade of UiO-66 research: a historic review of dynamic structure, synthesis mechanisms, and characterization techniques of an archetypal metal-organic framework. *Cryst Growth des.* 2019;20(2):1347-1362.
25. Myers AL, Prausnitz JM. Thermodynamics of mixed-gas adsorption. *AIChE J.* 1965;11(1):121-127.
26. Zlotea C, Phanon D, Mazaj M, et al. Effect of NH_2 and CF_3 functionalization on the hydrogen sorption properties of MOFs. *Dalton Trans.* 2011;40(18):4879-4881.
27. Kandiah M, Nilsen MH, Usseglio S, et al. Synthesis and stability of tagged UiO-66 Zr-MOFs. *Chem Mater.* 2010;22(24):6632-6640.
28. Yang SQ, Sun FZ, Liu P, et al. Efficient purification of ethylene from C_2 hydrocarbons with an C_2H_6/C_2H_2 -selective metal-organic framework. *ACS Appl Mater Interfaces.* 2021;13(1):962-969.
29. Wang Y, Hao C, Fan W, et al. One-step ethylene purification from an acetylene/ethylene/ethane ternary mixture by cyclopentadiene cobalt-functionalized metal-organic frameworks. *Angew Chem Int Ed Engl.* 2021;60(20):11350-11358.
30. Zhu B, Cao JW, Mukherjee S, et al. Pore engineering for one-step ethylene purification from a three-component hydrocarbon mixture. *J Am Chem Soc.* 2021;143(3):1485-1492.
31. Hao HG, Zhao YF, Chen DM, et al. Simultaneous trapping of C_2H_2 and C_2H_6 from a ternary mixture of $C_2H_2/C_2H_4/C_2H_6$ in a robust metal-organic framework for the purification of C_2H_4 . *Angew Chem Int Ed Engl.* 2018;57(49):16067-16071.
32. Xu Z, Xiong X, Xiong J, et al. A robust Th-azole framework for highly efficient purification of C_2H_4 from a $C_2H_4/C_2H_2/C_2H_6$ mixture. *Nat Commun.* 2020;11(1):3163.
33. Wang GD, Li YZ, Shi WJ, Hou L, Wang YY, Zhu Z. One-step C_2H_4 purification from ternary $C_2H_6/C_2H_4/C_2H_2$ mixtures by a robust metal-organic framework with customized pore environment. *Angew Chem Int Ed Engl.* 2022;134(28):e202205427.
34. Fan L, Zhou P, Wang X, Yue L, Li L, He Y. Rational construction and performance regulation of an In(III)-tetrakisophthalate framework for one-step adsorption-phase purification of C_2H_4 from C_2 hydrocarbons. *Inorg Chem.* 2021;60(14):10819-10829.
35. Jiang Z, Fan L, Zhou P, et al. An aromatic-rich cage-based MOF with inorganic chloride ions decorating the pore surface displaying the preferential adsorption of C_2H_2 and C_2H_6 over C_2H_4 . *Inorg Chem Front.* 2021;8(5):1243-1252.

SUPPORTING INFORMATION

Additional supporting information can be found online in the Supporting Information section at the end of this article.

How to cite this article: Liu J, Miao J, Wang H, Gai Y, Li J. Enhanced one-step purification of C_2H_4 from $C_2H_2/C_2H_4/C_2H_6$ mixtures by fluorinated Zr-MOF. *AIChE J.* 2023;e18021. doi:10.1002/aic.18021